

New Journal of Physics

The open access journal at the forefront of physics

Deutsche Physikalische Gesellschaft  DPG

IOP Institute of Physics

Published in partnership
with: Deutsche Physikalische
Gesellschaft and the Institute
of Physics



OPEN ACCESS

RECEIVED
22 December 2017

REVISED
21 March 2018

ACCEPTED FOR PUBLICATION
9 April 2018

PUBLISHED
4 May 2018

Original content from this
work may be used under
the terms of the [Creative
Commons Attribution 3.0
licence](#).

Any further distribution of
this work must maintain
attribution to the
author(s) and the title of
the work, journal citation
and DOI.



PAPER

Preferential weakening of rotational magnetic anisotropy by keV-He ion bombardment in polycrystalline exchange bias layer systems

Nicolas David Mügliche¹, Maximilian Merkel¹ , Alexander Gaul¹, Markus Meyl¹, Gerhard Götz², Günter Reiss², Timo Kuschel² and Arno Ehresmann¹

¹ Institute of Physics and Center for Interdisciplinary Nanostructure Science and Technology (CINSaT), University of Kassel, Heinrich-Plett-Straße 40, D-34132 Kassel, Germany

² Center for Spinelectronic Materials and Devices, Physics Department, Bielefeld University, Universitätsstraße 25, D-33615 Bielefeld, Germany

E-mail: max.merkel@physik.uni-kassel.de

Keywords: exchange bias, ion bombardment, rotatable anisotropy, unidirectional anisotropy, vector Kerr magnetometry, polycrystalline

Abstract

The consequences of keV light-ion bombardment of polycrystalline exchange bias layer systems on individual magnetic anisotropies composing the effective unidirectional magnetic anisotropy are investigated by vectorial magneto-optic Kerr effect measurements. Preferential reduction of rotatable magnetic anisotropy as compared to the other magnetic anisotropies is observable, disproving the intuitive assumption of an equal weakening of all magnetic anisotropies due to the bombardment. It is concluded that light-ion bombardment has a stronger impact on the magnetic characteristics of smaller grains in a polycrystalline antiferromagnet as compared to those of larger ones.

1. Introduction

Light-ion bombardment has proven to be a versatile and powerful technique to tailor magnetic characteristics of magnetic thin film systems [1–5] after their deposition. This technology is one among a few enabling the production of a multitude of functional elements in a large variety of applications [6–10]. In magnetoresistive sensor stacks (sensors based on the giant magnetoresistance effect or magnetic tunnel junctions) with magnetic reference electrodes pinned by exchange bias, for example, the pinning direction can be set to an arbitrary direction after completion of the deposition process essentially without changing the magnetoresistive effect amplitude [11–13]. Its possible use in creating magnetic logic elements has similarly been proven [14] as its potential to create engineered domain patterns by ion beam writing or when combined with lithographical techniques [1, 4, 15–17]. The latter patterns have shown to be useful for magnetic particle transport by moving domain walls [18], by changing potential energy landscapes associated with the stray fields above the engineered domains [19, 20] or by topological transport [21].

The two classes of layer systems most commonly used for modification by keV light-ion bombardment are polycrystalline Co/noble metal multilayers with an effective perpendicular-to-plane magnetic anisotropy and polycrystalline exchange bias layer systems with an effective in-plane magnetic anisotropy. Evidently the effective magnetic anisotropies in these layer systems result from a complex interplay of different individual magnetic anisotropies originating from interactions between layers or from the layers themselves [22–26]. Due to hyperthermal energy transfer from the ions into the layer system, implantation of ions, and defect creation the different prevailing magnetic anisotropies will be modified resulting in an altered effective magnetic anisotropy of the complete system. Whereas the modification of the effective magnetic anisotropies after keV light-ion bombardment is experimentally easily accessible and has been well characterized for a long time there are only reasonable conjectures how the different magnetic anisotropy contributions are individually affected by the impinging ions. As the effective magnetic anisotropy usually decreases with increasing ion fluence due to increased defect creation and ion implantation a likely supposition is that all magnetic anisotropy contributions of the layer system are decreased parallel to the decrease of the effective magnetic anisotropy. One exception is

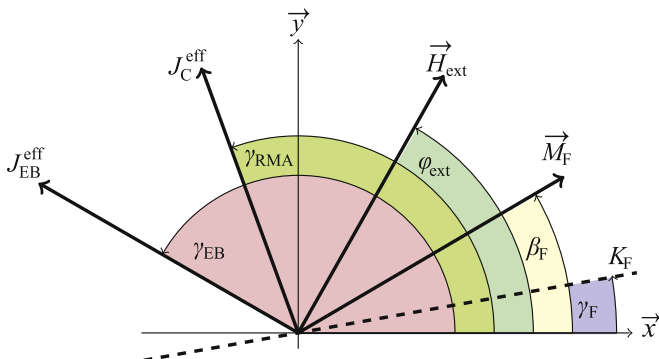


Figure 1. Illustration of angles and vectors for the used model in a polar coordinate system. \vec{M}_F is the magnetization vector of the ferromagnetic layer and β_F its azimuth. K_F is the energy density per unit volume of the ferromagnetic uniaxial magnetic anisotropy and γ_F the azimuth of its magnetic easy direction. \vec{H}_{ext} is the external magnetic field vector during the characterization measurements with the azimuth φ_{ext} . $J_{\text{EB}}^{\text{eff}}$ ($J_{\text{C}}^{\text{eff}}$) is the energy area density of the unidirectional magnetic anisotropy (rotatable magnetic anisotropy) with the corresponding azimuth γ_{EB} (γ_{RMA}). Reprinted figure with permission from [23], Copyright (2016) by the American Physical Society.

the increase of the exchange bias field in polycrystalline exchange bias layer systems, which may be also explained by a decrease of magnetic anisotropy in larger antiferromagnetic crystallites [22, 27–29]. Although experimental evidence for the modification of the individual magnetic anisotropies via keV light-ion bombardment exists [26], a quantitative disentanglement of the individual contributions, allowing a corresponding experimental proof of such a conjecture, is still missing.

In the present work we show that a recently developed model describing the effective unidirectional magnetic anisotropy in exchange bias layer systems by the different individual magnetic anisotropies can be used in conjunction with accurate measurements by vectorial magneto-optic Kerr effect (MOKE) magnetometry to identify effects of keV light-ion bombardment on the individual contributions. The investigations indicate that not all magnetic anisotropies in the layer system are reduced in the same way. The rotatable magnetic anisotropy prevailing in a certain class of smaller antiferromagnetic grains of the polycrystalline antiferromagnetic layer is reduced more dramatically than the other magnetic anisotropies in the system. This leads to the conclusion that keV light-ion bombardment does more efficiently modify the magnetic anisotropy associated with this class of grains. More generally our results indicate that the effects of light-ion bombardment on polycrystalline layer systems are grain size dependent. The results may initiate investigations to understand the physics fundamentals of the impact of light ions on individual material parameters of polycrystalline magnetic thin films rather than on averaged values.

2. Experimental

Exchange bias samples of the type Cu^{50nm}/Ir₁₇Mn₈₃^{30nm}/Co₇₀Fe₃₀^{15nm}/Si^{20nm} were fabricated on naturally oxidized Si including a field cooling procedure with a setting temperature of 573.15 K and an external magnetic field \vec{H}_{FC} of 80 kA m⁻¹ as done in [23]. Thereafter, samples were bombarded with 10 keV-He ions in a home built setup described in [30] under high vacuum conditions with a base pressure of 4×10^{-6} mbar. Ion bombardment (IB) was carried out with an ion current of approximately 10^{-6} A creating bombardment doses D ranging from 10^{13} to 10^{16} ions cm⁻². During IB an external magnetic field \vec{H}_{IB} of 70 kA m⁻¹ was applied either parallel or antiparallel to \vec{H}_{FC} . The two bombardment geometries will in the following be abbreviated by $\uparrow\uparrow$ IB and $\uparrow\downarrow$ IB, respectively.

Magnetization curves as a function of φ_{ext} , the angle between the direction of the external magnetic field applied for the characterization measurements and the arbitrarily chosen reference axis (\vec{x} in figure 1), were measured using vectorial MOKE magnetometry as described in [23, 31, 32]. In the setup longitudinal and transversal components of the magnetization are detected by analyzing polarization and intensity of the reflected light from a 632 nm diode laser, respectively. Magnetization curves were measured using 300 external magnetic field steps in a range of ± 80 kA m⁻¹ within 80 s. For each sample φ_{ext} was varied in the range of 0°–450° with a resolution of 1°. Absence of significant training effects was verified by comparing data from 0° to 90° with 360°–450°.

3. Model

For the numerical calculations the model of [23] was used whose main characteristics will be briefly summarized here. It is based on the coherent rotation approach introduced by Stoner and Wohlfarth [33, 34] calculating the angle of the ferromagnetic magnetization direction β_F with respect to the x -axis (see figure 1 for an overview of magnetic anisotropy and angle definitions). In the model the magnetic anisotropy of the ferromagnet was assumed to be uniaxial with the energy volume density K_F . The polycrystalline antiferromagnet was modeled by classifying its grains, exhibiting exchange interaction with the ferromagnet, in respect to their individual energy barriers ΔE_i distinguishing between a pinned and an unpinned state of the antiferromagnetic moment of the respective grain to the ferromagnetic magnetization [27]. The individual energy barriers can be expressed in first order by the product of the magnetic anisotropy $K_{AF,i}$ and the volume $V_{AF,i}$ of the grains. This allows the division based on the relaxation times of the grains

$$\tau_i = \tau_0 \exp\left[\frac{\Delta E_i}{k_B T}\right] \quad \text{with} \quad \Delta E_i = K_{AF,i} V_{AF,i}, \quad (1)$$

where $f_0 = 1/\tau_0$ is the characteristic frequency for spin reversal [35], T is the temperature and k_B is Boltzmann's constant. The grain size distribution of the antiferromagnet can be consequently connected to the distribution of relaxation times and is therefore commonly divided into four size classes with different thermal stability in comparison to the measurement conditions [22, 27, 36]. Small antiferromagnetic grains with corresponding energy barriers are thermally unstable during a magnetization reversal and can be divided into super-paramagnetic grains (Class I) and those having relaxation times in the order of the hysteresis duration (Class II) and therefore contributing to the coercivity of the system [22]. Thermally stable grains with relaxation times longer than the duration of the magnetization reversal are able to mediate the unidirectional anisotropy. Grains which can be set during field cooling conditions can yield a macroscopic contribution to the exchange bias (Class III), while grains with the highest energy barriers being stable during the field cooling procedure (Class IV) feature a random contribution to the direction of the unidirectional anisotropy.

The influence of the thermally unstable grains of Class II is modeled with a time-dependent rotatable magnetic anisotropy by considering an average relaxation time τ_{avg} for all grains of the corresponding class. The energy area density of the unidirectional and the rotatable magnetic anisotropy is J_{EB}^{eff} and J_C^{eff} , respectively, and is connected to the number of antiferromagnetic grains in each class. The total energy area density of a system with the sample surface A consisting of the potential energy of the ferromagnetic moment inside of the external magnetic field (Zeemann energy) E_Z and the anisotropy energies of the ferromagnetic uniaxial magnetic anisotropy (FUMA) E_{FUMA} , the unidirectional E_{UDA} and the rotatable magnetic anisotropy E_{RMA} is

$$\begin{aligned} E/A &= (E_Z + E_{FUMA} + E_{UDA} + E_{RMA})/A \\ &= -\mu_0 H_{ext} M_{sat} t_F \cos(\beta_F - \varphi_{ext}) \\ &\quad + K_F t_F \sin^2(\beta_F - \gamma_F) \\ &\quad - J_{EB}^{eff} \cos(\beta_F - \gamma_{EB}) \\ &\quad - J_C^{eff} \cos(\beta_F - \gamma_{RMA}) \\ \text{with } \gamma_{RMA} &= \beta_F(t - \tau_{avg}). \end{aligned} \quad (2)$$

Here, μ_0 is the magnetic permeability in vacuum, M_{sat} the saturation magnetization of the ferromagnet with thickness t_F . H_{ext} and φ_{ext} are strength and direction of the external magnetic field, respectively. γ_F , γ_{EB} and γ_{RMA} are the angles between the x -axis of the coordinate system and the magnetic easy directions of the FUMA, the unidirectional anisotropy, and the rotatable magnetic anisotropy, respectively (figure 1). While γ_F and γ_{EB} emerge from sample processing γ_{RMA} is connected to β_F via τ_{avg} with the time t [23].

4. Results

The exchange bias field $H_{EB}(\varphi_{ext})$ and the coercivity $H_C(\varphi_{ext})$ determined from vectorial MOKE measurements for different D (figure 2) show the modifications of the characteristic quantities H_{EB} and H_C of the investigated exchange bias layer systems by IB. $H_{EB}(\varphi_{ext})$ behaves roughly sinusoidal for all ion doses. The fine structure near the magnetic easy axis of the system ($\varphi_{ext} \approx 90^\circ$) leading to a deviation from the sine shape is caused by FUMA [23, 37, 38]. Small deviations from the mirror symmetry with respect to the magnetic easy axis can be attributed to a misalignment ($\leq 2^\circ$) between FUMA and the unidirectional magnetic anisotropy [39, 40]. For increasing ion dose D in the $\uparrow\downarrow$ IB case the amplitude of $H_{EB}(\varphi_{ext})$ is successively reduced until it reaches a maximum with opposite sign at about $D = 10^{15}$ ions cm^{-2} and is for higher doses reduced in magnitude. This is in accordance with previous magnetic easy axis hysteresis measurements [3, 41, 42]. Additionally, the fine structure near the magnetic easy axis of the system is reduced for higher ion doses until it vanishes. This first important result

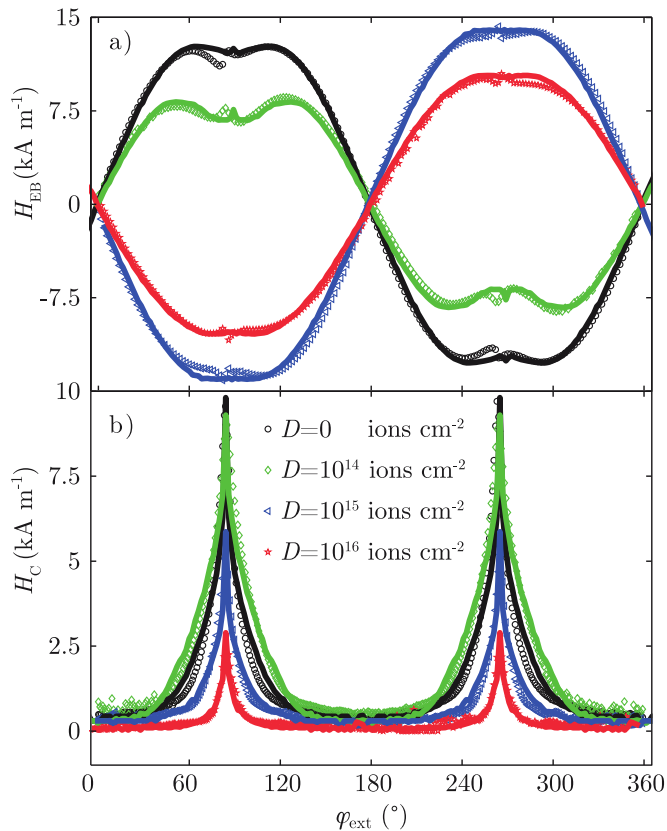


Figure 2. Experimentally determined (a) exchange bias field $H_{\text{EB}}(\varphi_{\text{ext}})$ and (b) coercivity $H_C(\varphi_{\text{ext}})$ for an exchange bias system of $\text{Cu}^{50\text{nm}}/\text{Ir}_{17}\text{Mn}_{83}^{30\text{nm}}/\text{Co}_{70}\text{Fe}_{30}^{15\text{nm}}/\text{Si}^{20\text{nm}}$ after $\uparrow\downarrow$ IB with different D . Solid lines correspond to a fit using equation (2).

indicates the individual response of the FUMA contribution to the present light-ion bombardment as a part of the modification of the total effective magnetic anisotropy of the layer system.

The experimentally determined relations $H_C(\varphi_{\text{ext}})$ show a lorentzian like shape indicating that coercivity results from a superposition of FUMA and rotatable magnetic anisotropy [23]. The peak height and width of $H_C(\varphi_{\text{ext}})$ is reduced with higher D .

Fitting the model parameters to the experimental data (solid lines in figure 2) enables the determination of material parameters as functions of D (figure 3). For the calculations M_{sat} was assumed to be dependent on the ion dose with

$$M_{\text{sat}} = \left(1230 - 5 \times 10^{-14} \cdot D \cdot \frac{\text{cm}^2}{\text{ions}} \right) \text{kA m}^{-1} \quad (3)$$

as derived in [5] for a similar exchange bias layer system. Solely $J_{\text{EB}}^{\text{eff}}$ as a function of D shows a dependence on the direction of \vec{H}_{IB} (figure 3(a)). In the $\uparrow\uparrow$ IB case $J_{\text{EB}}^{\text{eff}}$ is slightly increased for smaller D while it is more complex in the $\uparrow\downarrow$ IB case. Both relations agree with previous magnetic easy axis hysteresis measurements where H_{EB} was measured as a function of D [3, 28]. The small increase in the absolute value of $J_{\text{EB}}^{\text{eff}}$ at $D \approx 10^{15}$ ions cm⁻² is linked to a part of Class IV grains converted to Class III grains (figure 4(a)) [18, 27]. Due to the high energy transfer of the ions into the layer system some of these grains may overcome their relatively high energy barrier and relax into their energetically favored state. In this sense a number of grains are transferred by the IB from Class IV to Class III. The decrease of $J_{\text{EB}}^{\text{eff}}$ for higher ion doses of $D \approx 10^{16}$ ions cm⁻² is linked to a general decrease of the ferromagnet/antiferromagnet interaction as a consequence of interlayer intermixing [43]. The complexity of $J_{\text{EB}}^{\text{eff}}$ in the $\uparrow\downarrow$ IB case including the sign change is due to local field cooling induced by hyperthermal energy transfer. One should note that the macroscopic $J_{\text{EB}}^{\text{eff}}$ displays the coupling of the ferromagnetic magnetization to the vector sum of the microscopic antiferromagnetic moments. In this sense $J_{\text{EB}}^{\text{eff}}$ refers to the average exchange bias direction. Thus, in the $\uparrow\downarrow$ IB case, the directions of the microscopic exchange constants $J_{\text{F/AF},i}$ are changed. In contrast to previous magnetic easy axis hysteresis measurements showing perfectly the macroscopic modification of the effective unidirectional magnetic anisotropy [27], the angular resolved measurements clearly reveal that exchange bias reorientation takes place successively on a local basis correlated to the modification of individual grains representing a certain size class and not via coherent rotation.

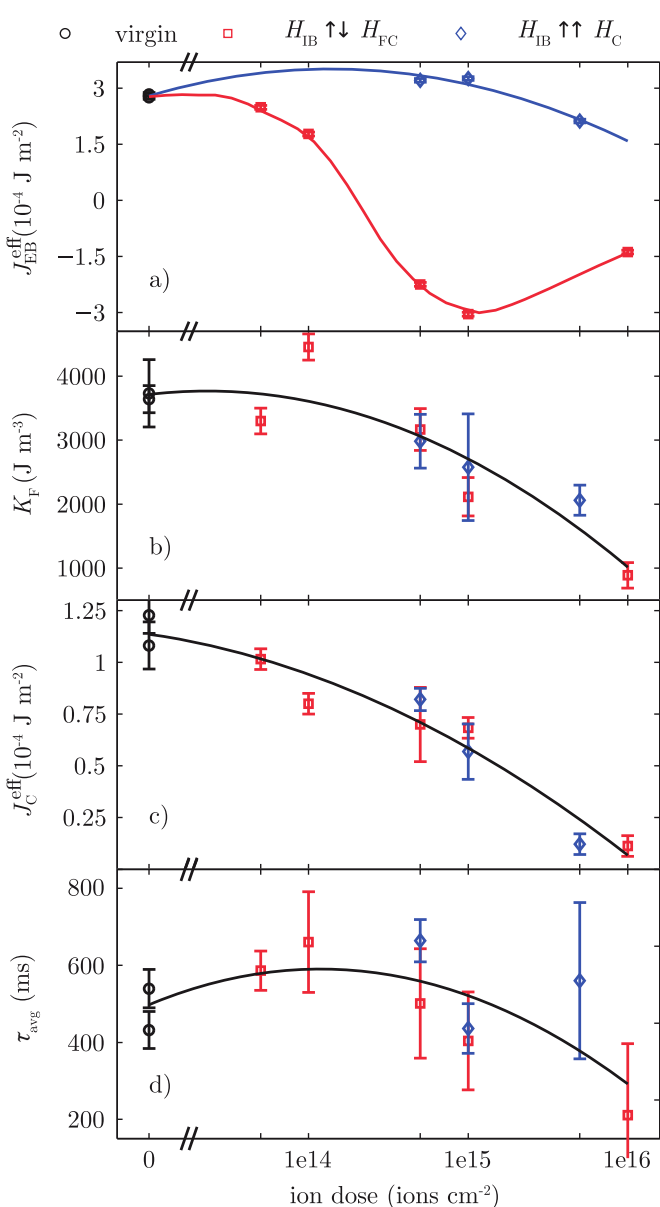


Figure 3. Characteristic quantities (a) J_{EB}^{eff} , (b) K_F , (c) J_C^{eff} and (d) τ_{avg} of the exchange bias layer as functions of D obtained by a fit of the model parameters to the experimental results $H_{EB}(\varphi_{ext})$ and $H_C(\varphi_{ext})$. Black circles belong to unbombarded, red squares and blue diamonds to bombarded samples in $\uparrow\downarrow$ IB and $\uparrow\uparrow$ IB configuration, respectively. The uncertainty in the fit parameters has been determined by a variation of the starting conditions. Lines are guides to the eye.

K_F as the characteristic quantity of FUMA shows a decrease for higher D and is reduced to roughly 25% for $D = 10^{16} \text{ ions cm}^{-2}$ as compared to the value for the unbombarded layer system (figure 3(b)) which is in qualitative agreement to previous studies involving a different material system [1]. The reduction of magnetic anisotropy can be attributed to the ion induced defect creation in the ferromagnetic layer leading to a decrease of crystalline order. K_F shows no dependence on the direction of \vec{H}_{IB} .

For J_C^{eff} and τ_{avg} , which are used to describe the thermally unstable grains of Class II, again, no influence of the bombardment field \vec{H}_{IB} direction on the dose dependency was detected (figures 3(c), (d)). This was suspected since the magnetic state is thermally unstable and the magnetic conditions during the field cooling or the bombardment process are not memorized. J_C^{eff} shows a massive decrease to only 10% for ion doses of $10^{16} \text{ ions cm}^{-2}$ as compared to the value of the unbombarded sample. For small ion doses τ_{avg} seems to increase slightly while it is not possible to determine a trend for higher ion doses due to the large uncertainty.

Summing up bombardment by light ions reduces the rotatable magnetic anisotropy much stronger than it modifies the unidirectional magnetic anisotropy. This is a counterintuitive result when assuming a statistical distribution of defects in all grains of the polycrystalline layer system. In first order, the energy densities of both, rotatable and unidirectional magnetic anisotropy, can be approximated as the product of the number of grains in Classes II and III, respectively, and the microscopic ferromagnet/antiferromagnet exchange interaction

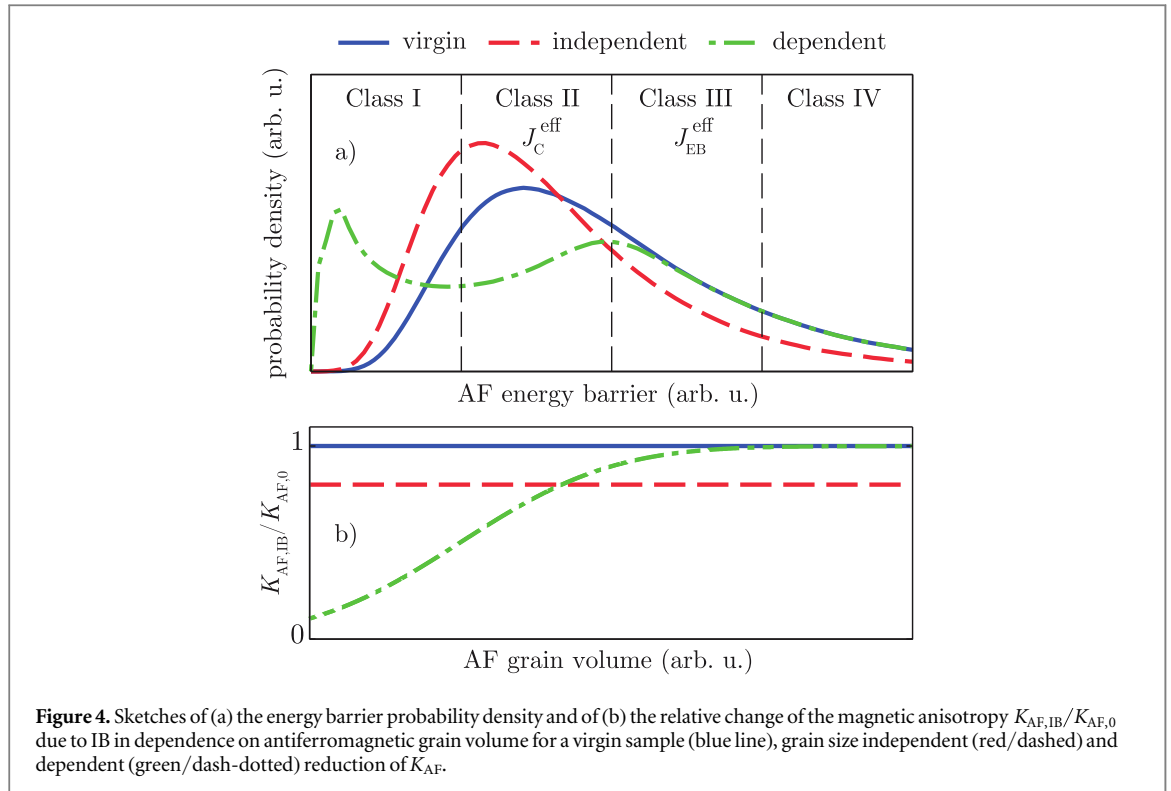


Figure 4. Sketches of (a) the energy barrier probability density and of (b) the relative change of the magnetic anisotropy $K_{AF,IB}/K_{AF,0}$ due to IB in dependence on antiferromagnetic grain volume for a virgin sample (blue line), grain size independent (red/dashed) and dependent (green/dash-dotted) reduction of K_{AF} .

constant $J_{F/AF,i}$ for grains i in contact to the ferromagnet. Both are altered by defect creation as IB not only decreases $J_{F/AF,i}$ but also the magnetic anisotropy of antiferromagnetic grains K_{AF} (and of the ferromagnet, as has been shown above) [27]. Thus, thermal stability of antiferromagnetic grains is changed by the bombardment process leading to different numbers of grains in each category.

If we now assume evenly distributed defects, $J_{F/AF,i}$ and K_{AF} should be reduced by a similar percentage for all grain sizes as the number of defects per unit volume is constant. For a lognormal antiferromagnetic grain size distribution the resulting distribution of energy barriers of antiferromagnetic grains in contact to the ferromagnet should be also lognormal (blue line in figure 4(a)). A grain size independent reduction of K_{AF} (dashed line in figure 4(b)) would modify this distribution towards lower energies (dashed line in figure 4(a)). Such a modified energy barrier distribution is not able to explain the dramatic decrease of J_C^{eff} relative to the modification J_{EB}^{eff} for higher D . This statement holds even if we would assume that all grains of Class IV would contribute to J_{EB}^{eff} as the number of unset grains at field cooling temperatures of 300 °C for an antiferromagnet with a Néel temperature of 400 °C should be rather low [22].

A grain size dependent reduction of K_{AF} would reduce the magnetic anisotropy of a large number of Class II grains to become superparamagnetic, whereas the magnetic anisotropy of larger grains is much less affected, not only explaining the massive decrease of J_C^{eff} , but also the increase of τ_{avg} for smaller ion doses as the average energy barrier of the remaining Class II grains is increased. The reason for this unexpected finding is not fully clear, however, we may hypothesize on it by two arguments: (1) smaller grains are thinner, i.e. their spatial extension orthogonal to the ferromagnet/antiferromagnet interface is smaller, which makes them prone to be more efficiently affected by intermixing. (2) Their proportion of surface with respect to bulk atoms is higher. At room temperature the chance of recombination after defect creation in bulk is 99% [44] so that most of the created defects vanish quickly. In case of surface atoms displaced atoms could be out of range for recombination reducing their chance of recombination.

5. Conclusions

In this work, we have determined the influence of keV-He ion bombardment on individual magnetic anisotropies of exchange bias systems quantitatively by fitting a coherent rotation model to experimental data obtained by vectorial MOKE magnetometry. The results show that ion bombardment induced modification of exchange bias takes place locally supporting the validity of the polycrystalline model of exchange bias. The reduction of coercivity caused by ion bombardment can be attributed to both a reduction of the ferromagnetic uniaxial magnetic anisotropy and the rotatable magnetic anisotropy. The fast decrease of rotatable magnetic anisotropy with increasing ion doses suggests that the reduction of magnetic anisotropy by light-ion

bombardment in the antiferromagnet is more prominent in smaller grains having a higher proportion of surface atoms and/or a smaller thickness. This excludes the intuitive assumption that ion bombardment causes an equitable weakening of all magnetic anisotropies. The result that in polycrystalline layer systems smaller grains are much more affected by statistically impinging ions may be the basis for revisiting phenomena associated with ion bombardment induced material modifications.

Acknowledgments

NDM thanks the University of Kassel for the Universität Kassel Promotionsstipendium.

ORCID iDs

Maximilian Merkel  <https://orcid.org/0000-0003-0789-1822>

Timo Kuschel  <https://orcid.org/0000-0002-9371-8876>

References

- [1] Chappert C *et al* 1998 Planar patterned magnetic media obtained by ion irradiation *Science* **280** 1919–22
- [2] Mewes T *et al* 2000 Suppression of exchange bias by ion irradiation *Appl. Phys. Lett.* **76** 1057–9
- [3] Mougin A *et al* 2001 Local manipulation and reversal of the exchange bias field by ion irradiation in FeNi/FeMn double layers *Phys. Rev. B* **63** 060409
- [4] Mougin A *et al* 2001 Magnetic micropatterning of FeNi/FeMn exchange bias bilayers by ion irradiation *J. Appl. Phys.* **89** 6606–8
- [5] Huckfeldt H *et al* 2017 Modification of the saturation magnetization of exchange bias thin film systems upon light-ion bombardment *J. Phys.: Condens. Matter* **29** 125801
- [6] Fassbender J, Ravelson D and Samson Y 2004 Tailoring magnetism by light-ion irradiation *J. Phys. D: Appl. Phys.* **37** 179–96
- [7] McCord J, Mönch I, Fassbender J, Gerber A and Quandt E 2009 Local setting of magnetic anisotropy in amorphous films by Co ion implantation *J. Phys. D: Appl. Phys.* **42** 055006
- [8] Devolder T *et al* 1999 Sub-50 nm planar magnetic nanostructures fabricated by ion irradiation *Appl. Phys. Lett.* **74** 3383–5
- [9] Yang Z P, Tan C L, Gao Z Y, Gao Y and Cai W 2017 Effect of proton irradiation on microstructural and magnetic properties of ferromagnetic Ni–Mn–Ga thin films *Thin Solid Films* **632** 10–6
- [10] Yang Z P, Gao Z Y and Cai W 2017 Proton-irradiation-induced structural and magnetic property changes in Ni–Mn–Ga high-temperature shape memory films *Mater. Sci. Eng. B* **223** 76–83
- [11] Engel D *et al* 2003 Alteration of exchange anisotropy and magnetoresistance in Co/Cu/Co/FeMn spin valves by ion bombardment *J. Appl. Phys.* **94** 5925–9
- [12] Schmalhorst J *et al* 2003 Influence of ion bombardment on transport properties and exchange bias in magnetic tunnel junctions *J. Appl. Phys.* **94** 5556–8
- [13] Höink V *et al* 2005 Postannealing of magnetic tunnel junctions with ion-bombardment-modified exchange bias *Appl. Phys. Lett.* **86** 15
- [14] Höink V *et al* 2007 Reconfigurable magnetic logic for all basic logic functions produced by ion bombardment induced magnetic patterning *Appl. Phys. Lett.* **91** 162505
- [15] Ehresmann A, Krug I, Kronenberger A, Ehlers A and Engel D 2004 In-plane magnetic pattern separation in NiFe/NiO and Co/NiO exchange biased bilayers investigated by magnetic force microscopy *J. Magn. Magn. Mater.* **280** 369–76
- [16] Kuswik P *et al* 2011 Colloidal domain lithography for regularly arranged artificial magnetic out-of-plane monodomains in Au/Co/Au layers *Nanotechnology* **22** 095302
- [17] Gaul A *et al* 2016 Engineered magnetic domain textures in exchange bias bilayer systems *J. Appl. Phys.* **120** 033902
- [18] Ehresmann A *et al* 2011 Asymmetric magnetization reversal of stripe-patterned exchange bias layer systems for controlled magnetic particle transport *Adv. Mater.* **23** 5568
- [19] Holzinger D, Koch I, Burgard S and Ehresmann A 2015 Directed magnetic particle transport above artificial magnetic domains due to dynamic magnetic potential energy landscape transformation *ACS Nano* **9** 7323–31
- [20] Ueltzhöffer T *et al* 2016 Magnetically patterned rolled-up exchange bias tubes: a paternoster for superparamagnetic beads *ACS Nano* **10** 8491–8
- [21] Loehr J *et al* 2017 Lattice symmetries and the topologically protected transport of colloidal particles *Soft Matter* **13** 5044–75
- [22] O’Grady K, Fernandez-Ooton L E and Vallejo-Fernandez G 2010 A new paradigm for exchange bias in polycrystalline thin films *J. Magn. Magn. Mater.* **322** 883–99
- [23] Mügliche N D *et al* 2016 Time-dependent rotatable magnetic anisotropy in polycrystalline exchange-bias systems: dependence on grain-size distribution *Phys. Rev. B* **94** 184407
- [24] Nicolodi S *et al* 2012 Negative rotatable anisotropy in IrMn/Cr/Co thin films *Phys. Rev. B* **85** 224438
- [25] Dias T *et al* 2014 Rotatable anisotropy driven training effects in exchange biased Co/CoO films *J. Appl. Phys.* **115** 243903
- [26] Schafer D *et al* 2015 Antiparallel interface coupling evidenced by negative rotatable anisotropy in IrMn/Fe bilayers *J. Appl. Phys.* **117** 215301
- [27] Ehresmann A, Junk D, Engel D, Paetzold A and Röll K 2005 On the origin of ion bombardment induced exchange bias modifications in polycrystalline layers *J. Phys. D: Appl. Phys.* **38** 801
- [28] Ehresmann A, Schmidt C, Weis T and Engel D 2011 Thermal exchange bias field drift in field cooled Mn₈₃Ir₁₇/Co₇₀Fe₃₀ thin films after 10 keV He ion bombardment *J. Appl. Phys.* **109** 023910
- [29] Schmidt C, Weis T, Engel D and Ehresmann A 2011 Thermal exchange bias field drifts after 10 keV He ion bombardment: storage temperature dependence and initial number of coupling sites *J. Appl. Phys.* **110** 113911
- [30] Lengemann D, Engel D and Ehresmann A 2012 Plasma ion source for *in situ* ion bombardment in a soft x-ray magnetic scattering diffractometer *Rev. Sci. Instrum.* **83** 053303

- [31] Kuschel T *et al* 2011 Vectorial magnetometry using magnetooptic Kerr effect including first-and second-order contributions for thin ferromagnetic films *J. Phys. D: Appl. Phys.* **44** 265003
- [32] Jiménez E *et al* 2014 Vectorial Kerr magnetometer for simultaneous and quantitative measurements of the in-plane magnetization components *Rev. Sci. Instrum.* **85** 053904
- [33] Stoner E C and Wohlfarth E P 1947 Interpretation of high coercivity in ferromagnetic materials *Nature* **160** 650–1
- [34] Stoner E C and Wohlfarth E P 1948 A mechanism of magnetic hysteresis in heterogeneous alloys *Phil. Trans. R. Soc.* **240** 599–642
- [35] Vallejo-Fernandez G, Aley N P, Chapman J N and O’Grady K 2010 Measurement of the attempt frequency in antiferromagnets *Appl. Phys. Lett.* **97** 222505
- [36] Soeya S, Fuyama M, Tadokoro S and Imagawa T 1996 NiO structure-exchange anisotropy relation in the $\text{Ni}_{81}\text{Fe}_{19}/\text{NiO}$ films and thermal stability of its NiO film *J. Appl. Phys.* **79** 1604–10
- [37] Xi H, Kryder M H and White R M 1999 Study of the angular-dependent exchange coupling between a ferromagnetic and an antiferromagnetic layer *Appl. Phys. Lett.* **74** 2687
- [38] Bai Y, Yun G and Bai N 2010 The jump phenomenon in the angular dependence of the off-aligned exchange bias *J. Appl. Phys.* **107** 033905
- [39] Jiménez E *et al* 2009 Highly asymmetric magnetic behavior in exchange biased systems induced by noncollinear field cooling *Appl. Phys. Lett.* **95** 122508
- [40] Jiménez E *et al* 2011 Role of anisotropy configuration in exchange-biased systems *J. Appl. Phys.* **109** 07D730
- [41] Juraszek J *et al* 2002 Tuning exchange bias and coercive fields in ferromagnet/antiferromagnet bilayers with ion irradiation *J. Appl. Phys.* **91** 6896–8
- [42] Engel D *et al* 2003 Exchange anisotropy modification in NiO/NiFe bilayers by ion bombardment *J. Magn. Magn. Mater.* **263** 275–81
- [43] Schmalhorst J, Sacher M D, Höink V, Reiss G, Engel D and Ehresmann A 2004 X-ray absorption and magnetic circular dichroism studies of ion-bombarded ferromagnet–antiferromagnet bilayers *Phys. Rev. B* **70** 184403
- [44] Ziegler J F, Biersack J P and Ziegler M D 2008 SRIM—*The Stopping and Range of Ions in Matter* (Chester, MD: SRIM) ch 7